Spatially Resolved Measurements of Metastable Atom Density and Electric Field Strength in a Microhollow Cathode Helium Plasma by Laser Absorption Spectroscopy*)

Keisuke UENO, Kenta KAMEBUCHI, Jiro KAKUTANI, Leo MATSUOKA[1)], Shinichi NAMBA[1)], Keisuke FUJII, Taiichi SHIKAMA and Masahiro HASUO

Graduate School of Engineering, Kyoto University, Katsura, Kyoto 615-8540, Japan
[1)]*Graduate School of Engineering, Hiroshima University, 1-4-1 Kagamiyama, Higashi-Hiroshima, Hiroshima 739-8527, Japan*

(Received 28 December 2017 / Accepted 10 April 2018)

We apply laser absorption spectroscopy to direct-current hollow-cathode helium plasma generated in a 0.3-mm-diameter cylindrical hole at gas pressures of 10 - 80 kPa. The measured transitions are 2^3S-2^3P and 2^1P-3^1D. We evaluate the helium metastable 2^3S density and gas temperature using the former transition and the 2^1P atom density and electric field strength from the latter one. The observed lateral distributions of the 2^3S and 2^1P atom densities depend on the gas pressure, which results from the sheath length estimated based on the spatial distribution of the evaluated electric field strength.

Keywords: microhollow cathode discharges, laser absorption spectroscopy, helium metastable

DOI: 10.1585/pfr.13.3406070

1. Introduction

Microhollow cathode discharge (MHCD) is a method for generating plasma at atmospheric pressure [1]. The main mechanism for sustaining the plasma is the back-and-forth motion (pendulum motion) of electrons that are emitted from the cathode wall and ionization by the accelerated electrons in the sheath region [2]. The typical gap voltage values between anode and cathode at cathode-hole diameters of smaller than 1 mm ranges between ~200 and 300 V [3–6].

The plasma parameters in MHCD have been estimated using the emission spectroscopy [3, 4], laser absorption spectroscopy [5,6] and numerical simulations [7]. Lazzaroni *et al*. obtained the two-dimensional images of the emission intensities of Ar $5p[3/2]_1$-$4s[3/2]_1$ (427.2 nm) and Ar^+ $4p'^2P_{3/2}$-$4s'^2D_{5/2}$ (427.8 nm) lines in 0.4-mm-diameter argon MHCD plasma in the pressure range of 4 - 27 kPa [3]. They indicated that the profile change of the two-dimensional image of the emission intensity with increasing background gas pressure is caused due to the reduction of the sheath length. Namba *et al*. observed a two-dimensional image of the emission intensity of He 2^1P-3^1D (667.8 nm) and Hα (656.3 nm) lines [4] in 1-mm helium MHCD plasma at 0.7 - 21 kPa. They observed that the emission intensity was localized to the cathode wall at pressures of greater than 7 kPa, a phenomenon that they attributed to the change of the mean free pass of inelastic collisions. Applying laser absorption spectroscopy on the He 2^3S-2^3P (1083 nm) transition in 0.3-mm helium MHCD plasma at 10 - 80 kPa [5], it was observed that the two-dimensional profile of the helium metastable (2^3S) became ring-shaped at a high pressure of greater than 60 kPa. Kothnur *et al*. performed a two-dimensional fluid simulation of 0.2-mm helium MHCD plasma at 40 and 133 kPa [7], and the results were qualitatively consistent with our previous experimental results [5]. Furthermore, the 2^1P atom density, n_{21P}, and electric field strength, E, were evaluated in 0.3-mm helium MHCD plasma at 10 kPa based on the laser absorption spectra of the 2^1P-3^1D [6].

However, the discharge voltage and the plasma parameters of the current results that are described in Sec. 3 are quantitatively different from those that were produced previously [5, 6] even though the discharge setup is the same in both the experiments. This is because the surface conditions of the electrode walls are observed to influence the discharge condition. Therefore, in this study, we measure the laser absorption spectra for the two transitions at an identical discharge condition. Further, we compare the pressure dependence of the two-dimensional images of the 2^3S atom density, n_{23S} and n_{21P}, from the two-dimensional profile of E.

2. Experimental Setup

Figure 1 depicts the experimental setup for the laser absorption spectroscopy and the cross sectional view of the electrodes. A 1-mm-thick ceramic insulator plate sep-

author's e-mail: ueno.keisuke.65m@st.kyoto-u.ac.jp
*) This article is based on the presentation at the 26th International Toki Conference (ITC26).

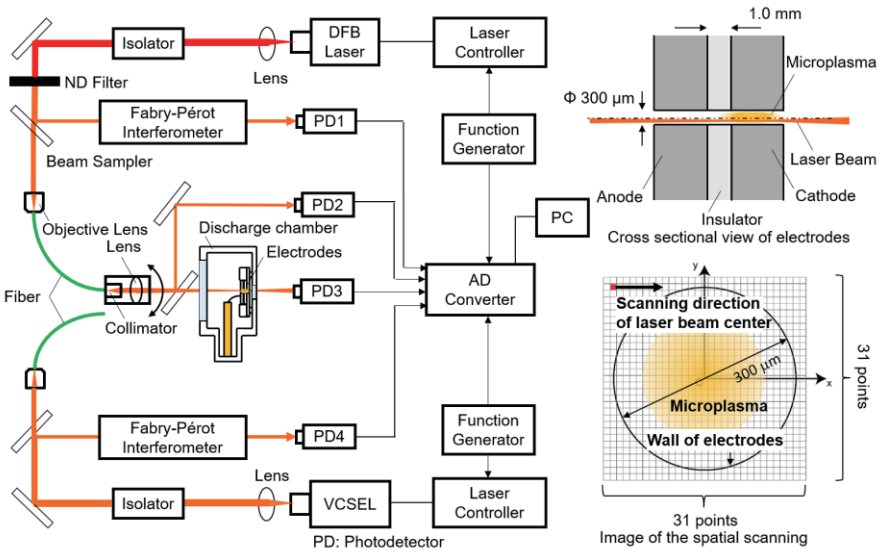

Fig. 1 The experimental setup.

arated a 2-mm-thick cathode and anode, each with a 0.3-mm-diameter discharge hole in its center. The discharge chamber was filled with helium gas, and plasma was generated by a direct-current voltage. We set a discharge current of 15 mA under all the gas pressure conditions, and the measured voltages between the cathode and anode were 220, 230, 230, 220, and 200 V at gas pressures of 10, 20, 40, 60, and 80 kPa, respectively. The laser light sources were distributed-feedback (DFB) diode laser (Toptica LD-1083-0070-DFB-1) and vertical-cavity surface emitted diode laser (VCSEL) (Vixar V670S-002-0001) for the 2^3S-2^3P and 2^1P-3^1D transition measurements, respectively. We scanned the light frequency by varying the injection current to the laser diode, which was accomplished by applying a 100 Hz triangular-wave voltage from a function generator (Agilent 33220A) to the laser controller (Arroyo Instruments ComboSource6300). Part of the laser beam is separated using a beam sampler to monitor the light frequency by Fabry-Pérot interferometers using photodetectors (PD1 or PD4). The main beam was transmitted through an optical fiber. Part of the output beam from the optical fiber was separated using another beam sampler to monitor the incident light intensity, I_0, with a photodetector (PD2). The rest of the beam was focused on the discharge hole, and the transmitted light intensity, I, was measured using a photodetector (PD3). The measured diameters of the laser beams at the focal points were 55 and 27 μm in the Rayleigh criterion for the DFB laser and VCSEL, respectively. As depicted in the right-bottom image of Fig. 1, we scanned the lateral position of the focal point over the discharge hole with a spatial step of 9.9 μm by tilting the actuator-attached fiber holder. The measurements for the two transitions were conducted separately at the same discharge condition.

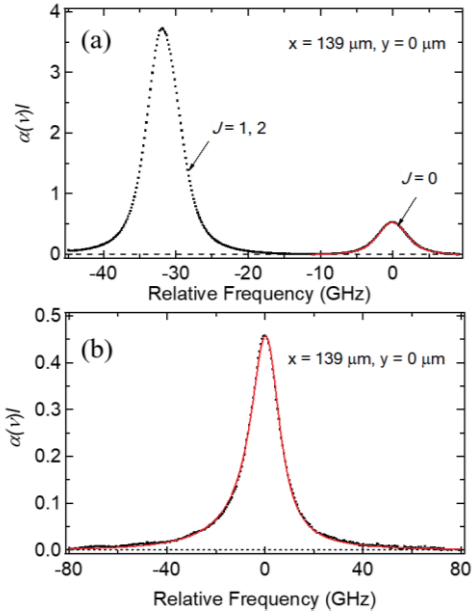

Fig. 2 The observed spectra of the 23S-23P transition measured at $(x, y) = (0\,\mu\text{m}, 0\,\mu\text{m})$ (a), and the 2^1P-3^1D transition measured at $(x, y) = (139\,\mu\text{m}, 0\,\mu\text{m})$ (b) at 40 kPa.

3. Results and Discussion

Figures 2 (a), (b) depict the absorption spectra, $\kappa = -\ln(I/I_0)$, of the 2^3S-2^3P and 2^1P-3^1D transitions, respectively, at the position $(x, y) = (139, 0\,\mu\text{m})$ at 40 kPa. The spectrum of the 2^3S-2^3P transition exhibits fine structure for the upper energy levels of 2^3P_J ($J = 0, 1, 2$). Because the spectra of $J = 1, 2$ are superposed and are saturated at some positions, we fit only the $J = 0$ spectrum using a Voigt function. The adjustable parameters for the fitting are the area of the spectrum, S_1, the Lorentz width, Δ_L, and the Doppler width, Δ_D. The fitting result is indicated with a red curve in Fig. 2. We evaluate $n_{23\text{S}}$ from S_1 and

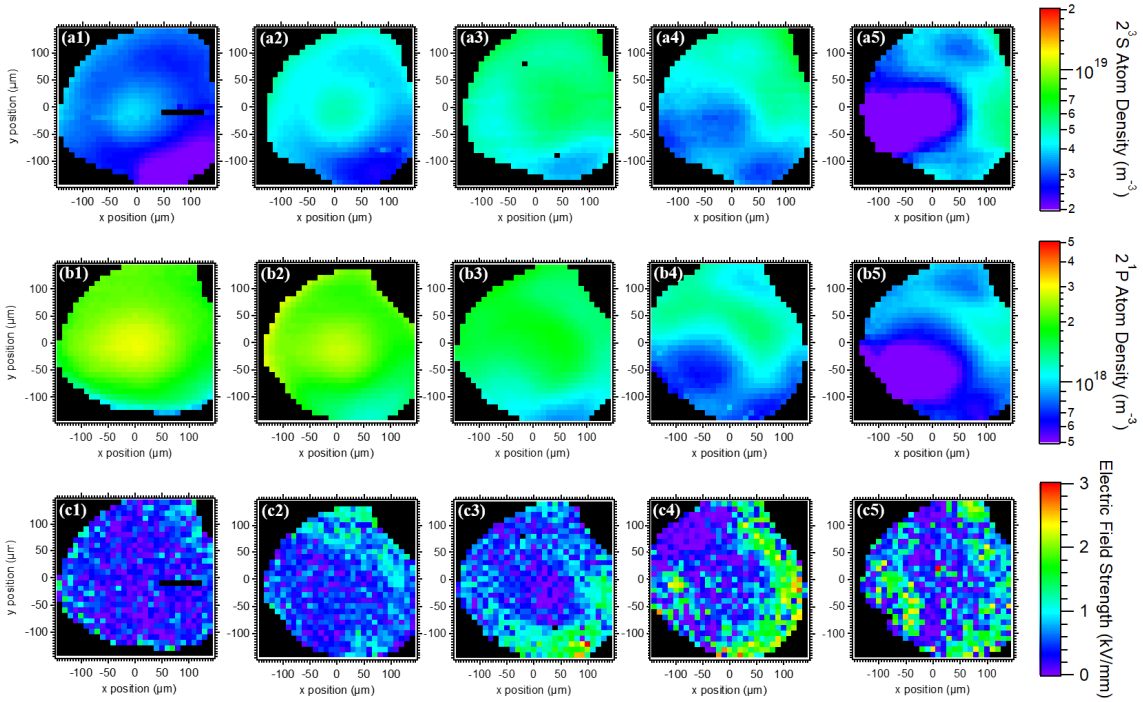

Fig. 3 Two-dimensional maps of the 2^3S atom density (a1) - (a4), the 2^1P atom density (b1) - (b4), and the electric field strength (c1) - (c4), at 10, 20, 40, 60, and 80 kPa, respectively.

the gas temperature T_g from Δ_D [5]. Here, we assume the absorption length to be 4 mm based on the thickness of the electrodes.

The observed absorption spectrum of the 2^1P-3^1D transition is asymmetric due to the Stark splitting of the 3^1D level [8]. We fit the spectrum with a Voigt function considering the Stark splitting [6]. The adjustable parameters for the fitting are the area of the spectrum, S_2, the Stark width, Δ_S, and the electric field strength, E, and its first derivative of space at the center of the laser light spot [6]. We evaluate n_{21P} from S_2 and the electron density n_e from Δ_S. Here, the Doppler widths of the 2^1P-3^1D spectrum are equal to the results that were obtained by multiplying ν_s/ν_t ($\nu_{s,t}$ are the transition frequencies of the 2^1P-3^1D and 2^3S-2^3P, respectively) with the Doppler width that was evaluated from the corresponding 2^3S-2^3P spectrum at each spatial point.

Figures 3 (a1) - (a5), (b1) - (b5), and (c1) - (c5) depict the two-dimensional maps of n_{23S}, n_{21P}, and E, respectively, at 10 - 80 kPa. The transmitted signal or the absorption is too low in the black area. From 10 to 40 kPa, n_{23S} and n_{21P} exhibit peaks at the center. The values of E are smaller than 1.0 kV/mm in almost the entire measured area at 10 and 20 kPa; however, E is relatively large near the cathode wall at 40 kPa. At 60 and 80 kPa, a hole appears in the structure of n_{23S} and n_{21P} near the center, and E near the cathode wall becomes larger than 2.0 kV/mm.

The observed change of E may be due to the shrinking sheath length. The electrons emitted from the cathode surface gain energy by the sheath electric field contribute to the excitation and ionization. The excitation energies from the ground state level to the 2^3S and 2^1P levels are 19.82 and 21.22 eV, respectively, and the ionization energy of helium is 24.59 eV [9]. The electrons generated by the ionizations are also accelerated toward the center, and they contribute to the excitation or ionization. The central peaks of n_{23S} and n_{21P} at 10 - 40 kPa are due to the large sheath lengths (>~50 - 100 μm estimated from the spatial distribution of E at 40 kPa). However, the high-density regions at 60 and 80 kPa are located near the cathode wall because of the short sheath length (<~50 μm) and the low electron energy at the center [7]. Lazzaroni *et al.* suggested that the peak position of the observed emission intensity from cathode wall changes due to the changes in the position of the sheath edge [3], and this is consistent with our results.

From the two-dimensional maps, the pressure at which the peak value is maximized and the location of the peak point is not clear. Therefore, we depict the values of n_{23S} and n_{21P} at the center (x, y) = (0, 0 μm) at 10, 20, and 40 kPa in Fig. 4 using red lines. Furthermore, we recognize that the peak value of n_{23S} in the center region is the highest at 40 kPa and that of n_{21P} is the highest at 10 kPa.

We calculate the electron energy distribution function (EEDF) using the Boltzmann equation solver BOLSIG+ [10] at 10, 20, and 40 kPa by setting the reduced electric field value (E/N) (N is the helium atom density), the gas temperature, and the electron collision cross sections. We set E at 1.0 kV/mm and the gas temperatures as (x, y) = (119, 0 μm) at 10, 20, and 40 kPa (depicted in Fig. 5). We use the cross-section data of the elastic collision, excita-

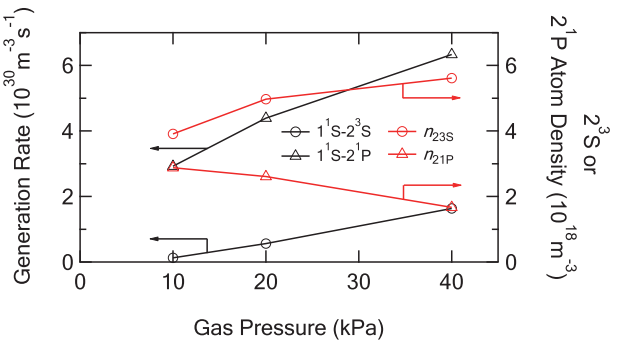

Fig. 4 The calculated generation rates of the 2^3S and 2^1P states, and n_{23S} and n_{21P} at (x, y) = (0, 0 μm) at 10, 20, and 40 kPa, respectively.

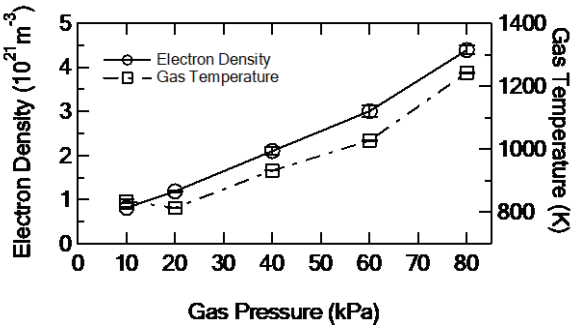

Fig. 5 The electron density and gas temperature evaluated at the spatial point (x, y) = (119, 0 μm) at all the gas pressure conditions.

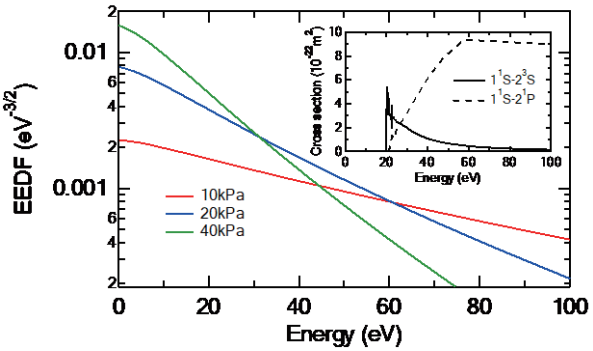

Fig. 6 The electron energy distribution function at 10, 20, and 40 kPa. The inset is the cross-section data of the 1^1S-2^3S and 1^1S-2^1P excitations.

tions from the ground level, and ionization from the Biagi v8.9 database [11]. Only the cross-sections of the excitations from ground state to the 2^3S and 2^1P states are depicted in the inset of Fig. 6. The calculated results of the EEDF are depicted in Fig. 6. Additionally, we calculate the generation rates of the 2^3S and 2^1P states using the following equation:

$$G = Nn_e \int_0^\infty \sigma(E_e) f(E_e) v \sqrt{E_e} dE_{e'}, \quad (1)$$

where n_e is the electron density, E_e is the electron energy, σ is the cross-section of the excitations, f is the EEDF defined as $\int_0^\infty f(E_e)\sqrt{E_e}dE_e = 1$, and v is the electron velocity. The values of G are depicted by the black lines in Fig. 4. It is observed that the values of G of the 2^3S or 2^1P states at 40 kPa are 13 or 2.2 times larger than those at 10 kPa, whereas the values of n_{23S} or n_{21P} at 40 kPa are 1.4 or 0.58 times larger than those at 10 kPa, respectively. The differences in the pressure dependences between G and the densities may result from differences in the pressure dependences of the quenching lifetimes of the 2^3S and 2^1P atoms.

Figure 5 also depicts n_e at (x, y) = (119, 0 μm). Although we do not depict the two-dimensional maps, the spatial distributions of n_e and T_g are approximately uniform. The values of n_e are 10^{20} - 10^{21} m^{-3} and become larger as the pressure increases. The observed pressure dependences of n_e and T_g are consistent with the results of the emission spectroscopy [4].

4. Conclusion

We performed laser absorption spectroscopy on microhollow cathode helium plasma with a diameter of 0.3 mm and evaluated the two-dimensional maps of the 2^3S and 2^1P atom densities, the electric field strength, the electron density, and the gas temperature. It was indicated that the change of the 2^3S and 2^1P atom densities with increasing pressure was caused due to the shrinking sheath length.

Acknowledgments

This work was partly supported by JSPS KAKENHI Grant-in-Aid for Challenging Exploratory Research (No.15K13607) and the Kansai Research Foundation for technology promotion (No. 2015R035).

[1] K.H. Schoenbach *et al.*, J. Vac. Sci. Technol. A **21**, 1260 (2003).
[2] G.J. Kim and J.K. Lee, IEEE Trans. Plasma Sci. **36**, 1238 (2008).
[3] C. Lazzaroni *et al.*, J. Phys. D **43**, 124008 (2010).
[4] S. Namba *et al.*, J. Appl. Phys. **110**, 073307 (2011).
[5] K. Ueno *et al.*, Jpn. J. Appl. Phys. **17**, 01AA03 (2018).
[6] K. Torii *et al.*, Plasma Fusion Res. **10**, 3406063 (2015).
[7] P.S. Kothnur and L.L. Raja, J. Appl. Phys. **97**, 043305 (2005).
[8] A.G. Frank *et al.*, J. Phys. B **39**, 5119 (2006).
[9] Atomic Spectra Database, ver.5, https://www.nist.gov/pml/atomic-spectra-database
[10] G.J. Hagelaar *et al.*, Plasma Sources Sci. Technol. **14**, 722 (2005), www.bolsig.laplace.univ-tlse.fr.
[11] Biagi- v8.9 database (Extracted from the Fortran code Magboltz, ver 8.9), www.lxcat.laplace.univ-tlse.fr.